Nearly total absorption of light and heat generation by plasmonic metamaterials

Jiaming Hao,[1] Lei Zhou,[2] and Min Qiu[1,3,*]

[1]*Laboratory of Photonics and Microwave Engineering, School of Information and
Communication Technology, Royal Institute of Technology (KTH), Electrum 229, Kista S-164 40, Sweden*
[2]*State Key Laboratory of Surface Physics and Physics Department, Fudan University, Shanghai 200433, China*
[3]*State Key Laboratory of Modern Optical Instrumentation and Institute of Advanced Nanophotonics, Department of Optical Engineering,
Zhejiang University, Hangzhou 310027, China*

We theoretically and numerically study the absorption effect and the heat generation in plasmonic metamaterials under light radiation at their plasmonic resonance. Three different types of structures, all possessing high-performance absorption for visible lights, are investigated. The main aim of this work is to present an intuitive and original understanding of the high-performance absorption effects. From the macroscopic electromagnetic point of view, the effective-medium approach is used to describe the absorption effects of the plasmonic metamaterials. On the other hand, the field distributions and heat generation effects in such plasmonic nanostructures are investigated, which also provides a satisfactory qualitative description of such absorption behavior based upon the microscopic perspective.

I. INTRODUCTION

The study of blackbody radiation ultimately led to the emergence of quantum mechanics over a century ago.[1,2] A blackbody is an ideal absorber that soaks up all the electromagnetic radiation that illuminates it. No radiation passes through it and none is reflected. The "bodies" with high absorption properties are of much importance at present in many fields of science and technology. For example, perfect absorbers can be used as photodectors,[3–5] microbolometers,[6] thermal images,[7] and absorbers and emitters for the thermal-photovoltaic solar energy conversion.[8–12] It has been shown that for an ideal microbolometer, photons that strike on their surfaces would be absorbed efficiently and converted to heat, then detected.[6] Perfect absorbers with narrow band absorption properties also have great significant application in thermal imaging. In the midinfrared frequency regime, single-pixel imaging has been demonstrated by a frequency- and spatially selective absorber.[7] One of the most important applications of the perfect absorber is in the field of thermal-photovoltaic solar energy conversion.[8–13] The perfect absorbers with broad spectrum features or narrow band responses are both necessary.[13] The former possesses blackbodylike behaviors and can be utilized to absorb solar energy effectively from the infrared frequency regime to the visible frequency regime. The latter is a selective emitter, which displays strong emission in the desired frequency region where narrow band gap photovoltaic cells could convert photons to electricity.[10,13] For these purposes, the nanostructures with high-performance absorption properties have been studied by many researchers. For example, more than 10 years ago, F. J. García-Vidal *et al.*[14] predicted that the low-density aligned carbon nanotube array can exhibit an extremely low refractive index. The light impinging on the surface of the carbon nanotube array is not reflected but rather absorbed by such medium strongly. Recently, an extremely dark material has been truly realized using such a carbon nanotube film.[15] V. G. Kravets *et al.*[16] in 2008 showed that plasmonic structures consisting of gold stripes combined with polymethyl methacrylate nanostripes

exhibit almost complete absorption in a wide optical wavelength range (240–550 nm) over a large range of incident angles. While the high absorption was limited to one light polarization with electric field vector perpendicular to the grating stripes, the reflection for the light with electric field vector directed parallel to the grating stripes is analogous to that from the plain gold film. Quite recently, they also proposed a plasmonic blackbody consisting of silver nanoparticles embedded in a dielectric matrix; this structure permits a high level of absorption above 90% of unpolarized light in a wide range of incident angles with an optical spectrum 240–850 nm.[17–19] The absorption of light with narrow band responses has also been investigated. At the beginning of last century, R. W. Wood[20] successively found abnormal optical absorption in metallic diffraction gratings and the structures composed by alkali metals deposited on a cold glass wall. It was demonstrated later that this effect should be dominated by the resonant excitation of surface plasmon polaritons.[21,22] Other routes to produce high-performance nanostructure absorbers are to use plasmonic photonic crystals,[23,24] periodic metallic structures,[25–28] in which these absorption effects are also dependent on the excitation of some kinds of resonances, like Bragg, Rayleigh resonances or plasmons both propagating and localized. Another kind of ideal candidate for realizing perfect absorber is a metamaterial.[7,29–38] The ability of metamaterials to possess any electromagnetic responses in nearly arbitrary frequencies has made it a hot research topic in recent years.[39,40] Recently we presented both theoretically and experimentally an ultrathin, wide-angle, subwavelength, high-performance metamaterial absorber for optical communication frequency.[41] The physical mechanism of the absorption effect is governed by the excitation of localized electromagnetic resonances.

Assume that the total energy of incident light would only to be reflected (*R*), transmitted (*T*), or absorbed (*A*); that is, $1 = R + T + A$. The idea of making absorption as large as possible is equal to decreasing both the reflectance and the transmittance. When the impedances of the plasmonic structures are perfectly matched to the free space impedance, no energy of incident light will be reflected, and optical resonances would be

stimulated. If the structures are thick enough, such resonances can trap light energy efficiently and provide sufficient time to dissipate it by the dielectric or Ohmic losses; that is, the light is absorbed and, consequently, converted into dissipated heat. The generation of heat in plasmonic structures induced by light absorption has also attracted much attention recently.[42–50] All applications above mentioned on the light absorption are always strongly related to the releasing heat process. In addition, the nanoscale control of optical heating based on the plasmonic nanostructures gave rise to a great number of new phenomena and promising applications, ranging from nanometer-sized heat source,[42–44] nanoscale fluidics,[45] radiation nanocatalysis,[46] photothermal cancer therapy,[47,48] inducing phase transitions,[49] and morphology optimization for nanostructures.[50] In this paper, we present three kinds of plasmonic metamaterial absorbers. All of them work in the at visible frequency regime. In order to illustrate the underlying physics of such high-performance absorption effects, we not only extract effective electromagnetic parameters for the plasmonic systems from the macroscopic electromagnetic point of view, but also investigate the field distributions and resistive heat in such plasmonic nanostructures based upon the microscopic perspective.

The paper is organized as follows. In Sec. II we discuss the general heat loss formula in a dispersive and absorptive material based on the law of conversion of electromagnetic energy. In Sec. III we present three kinds of metamaterial absorbers for visible frequencies and discuss their underlying mechanisms from both macroscopic and microscopic perspectives. For the second kind of metamaterial absorber, we also investigate the relationship between the absorption spectrum and the geometric dimensions of nanostructure to illustrate how to design such a high-performance absorber with a set of practical parameters. Finally, the conclusion is given.

II. HEAT LOSS IN A DISPERSIVE AND ABSORPTIVE MATERIAL

In this section, based on the law of conversion of electromagnetic energy, the so-called Poynting's theorem,[51] we study the losses associated with a light passing through a medium, in which both the dielectric permittivity and magnetic permeability are dispersive and absorptive.[52]

For a dispersive and absorbing medium, under the action of electric field, the equation of motion of the electric polarization can be expressed as[51]

$$\frac{\partial^2 \vec{P}}{\partial t^2} + \gamma_e \frac{\partial \vec{P}}{\partial t} + \omega_{eo}^2 \vec{P} = \varepsilon_0 \omega_{ep}^2 \vec{E}, \quad (1)$$

where γ_e is the damping constant, ω_{eo} is the binding or resonance frequency, and ω_{ep} is the plasma frequency measuring of the strength of the interaction between the oscillators and the electric field. Assume the material medium is characterized by the following constitutive relation: $D = \varepsilon_0 \vec{E} + \vec{P} = \varepsilon_0 \varepsilon \vec{E}$; here ε denotes the relative dielectric permittivity of the medium. Under the harmonic field excitation with time dependence $e^{-i\omega t}$, we have

$$\varepsilon(\omega) = 1 - \frac{\omega_{ep}^2}{\omega^2 - \omega_{eo}^2 + i\gamma_e \omega}, \quad (2)$$

which is in accordance with the Lorentz model.[51] When $\omega_{eo} = 0$, the above model will reduce to the Drude model. It is actually the common model to be used to describe the permittivity of realistic dispersive materials, such as ordinary dielectric media, metals, etc.

Similarly, in the presence of an oscillating magnetic field, the equation of motion of the magnetic polarization can be written as[52]

$$\frac{\partial^2 \vec{M}}{\partial t^2} + \gamma_m \frac{\partial \vec{M}}{\partial t} + \omega_{mo}^2 \vec{M} = \omega_{mp}^2 \vec{H}, \quad (3)$$

where γ_m and ω_{mo} are the damping constant and the resonance frequency of the magnetic oscillators, respectively. ω_{mp} is the magnetic plasma frequency measuring of the strength of the interaction between the oscillators and the magnetic field. Using the relation $\vec{B} = \mu_0(H + M) = \mu_0 \mu \vec{H}$, the relative magnetic permeability can be easily written in the form

$$\mu(\omega) = 1 - \frac{\omega_{mp}^2}{\omega^2 - \omega_{mo}^2 + i\gamma_m \omega}. \quad (4)$$

From the Maxwell's equation, one can easily obtain the Poynting's theorem in the integral form as

$$\int_{\sigma} (\vec{E} \times \vec{H}) \cdot d\vec{\sigma} = -\int_{V} \left(\vec{E} \cdot \frac{\partial \vec{D}}{\partial t} + \vec{H} \cdot \frac{\partial \vec{B}}{\partial t} \right) dV, \quad (5)$$

where σ is the closed surface surrounding the volume V and the vector $\vec{S} = \vec{E} \times \vec{H}$ is known as Poynting vector representing the energy flow, and has the dimensions of (Watts/m^2). Here we remove the term $-\int_{V} J \cdot E \, dV$ from the right-hand side of Eq. (5) because the contribution of conduction current has been regarded as part of the dielectric response.[51] Using Eqs. (1) and (3), one can rewrite Eq. (5) as

$$-\int_{V} \frac{\partial u}{\partial t} dV = \int_{\sigma} (\vec{E} \times \vec{H}) \cdot d\vec{\sigma} + \int_{V} \left(\frac{\gamma_e}{\varepsilon_0 \omega_{ep}^2} \left| \frac{\partial \vec{P}}{\partial t} \right|^2 \right. $$
$$\left. + \frac{\mu_0 \gamma_m}{\omega_{mp}^2} \left| \frac{\partial \vec{M}}{\partial t} \right|^2 \right) dV, \quad (6)$$

where u is total energy density and defined by

$$u = \frac{1}{2}\varepsilon_0 |E|^2 + \frac{1}{2}\mu_0 |H|^2 + \frac{1}{2\varepsilon_0 \omega_{ep}^2} \left(\left| \frac{\partial \vec{P}}{\partial t} \right|^2 + \omega_{eo}^2 |P|^2 \right) $$
$$+ \frac{\mu_0}{2\omega_{mp}^2} \left(\left| \frac{\partial \vec{M}}{\partial t} \right|^2 + \omega_{mo}^2 |M|^2 \right), \quad (7)$$

which includes both the electric and the magnetic parts.[52] The second term on the right-hand side of Eq. (6) represents the *absorptive dissipation* in the medium, in which both the electric energy loss and the magnetic energy loss are included. The physical meaning of the integral equation (6) is that the energy flowing out through the boundary surfaces of the volume V per unit time plus the rate of energy loss by absorptive dissipation in the volume is equal to the negative of the time rate of change of electromagnetic energy within the volume. Equation (6) displays the conservation of electromagnetic energy in the realistic situations.

Based on Eqs. (1)–(4), the time-averaged dissipative energy density can be rewritten as

$$q = q_e + q_m = \left\langle \frac{\gamma_e}{\varepsilon_0 \omega_{ep}^2} \left| \frac{\partial \vec{P}}{\partial t} \right|^2 + \frac{\mu_0 \gamma_m}{\omega_{mp}^2} \left| \frac{\partial \vec{M}}{\partial t} \right|^2 \right\rangle$$

$$= \frac{1}{2} \varepsilon_0 \omega \mathrm{Im}\varepsilon(\omega) |E|^2 + \frac{1}{2} \mu_0 \omega \mathrm{Im}\mu(\omega) |H|^2. \tag{8}$$

In the case of no magnetically dispersive medium, this reduces to

$$q = q_e = \frac{1}{2} \varepsilon_0 \omega \mathrm{Im}\varepsilon(\omega)|E|^2. \tag{9}$$

Equation (9) indicates that the electric energy loss density is proportional to working frequency, the imaginary part of permittivity of the medium, and the square of the total electric field amplitude.[53]

III. METAMATERIAL ABSORBER FOR VISIBLE FREQUENCIES

A. Small patches working around their first resonance frequency

We now study the first kind of perfect metamaterial absorber with its operating wavelength in the visible frequency regime. To begin with, we investigate the wave scattering properties by this variety of absorber to discuss the validity of the formula

$$A = 1 - R - T, \tag{10}$$

used to calculate the absorption.

As shown in Fig. 1, the concerned metamaterial absorber structure consists of three layers. The top layer is made of an array of silver particles and the bottom layer is a continuous silver film. A thin dielectric layer separates the two metallic layers as a spacer. The structure is assumed to be fabricated on a quartz substrate. The thickness of the rectangular metallic particle is denoted by t and its side lengths along the different axis are assumed to be W_x and W_y. The thicknesses of the dielectric layer and the silver film are represented by d and h, respectively. The lattice constant is denoted by a. The refractive index of the dielectric (Al_2O_3) is 1.75. The permittivity of silver is given by Drude model with the plasma frequency $\omega_p = 1.37 \times 10^{16} s^{-1}$ and the collision frequency $\gamma = 8.5 \times 10^{13} s^{-1}$. At the wavelength of interest here this model is adequate description of the actual refractive index of silver.[54] All materials were assumed to be nonmagnetic ($\mu = \mu_0$).

After some numerically computational efforts based on the finite-difference-time-domain method,[55] the optimized parameters for a perfect metamaterial absorber with operating wavelength near 600 nm are taken as $W_x = W_y = 50$ nm, $t = 30$ nm, $d = 12$ nm, $h = 80$ nm, and $a = 250$ nm. Except for the reflection (R), transmission (T), and absorption (A), one intuitively believes that there should exist strongly high-order scatterings (S), because the operating wavelength is merely two times larger than the lattice constant of the nanostructure. Here we define the attenuation of light as $Q_{att} = 1 - R - T$, in which both the absorbed and the scattered energy are
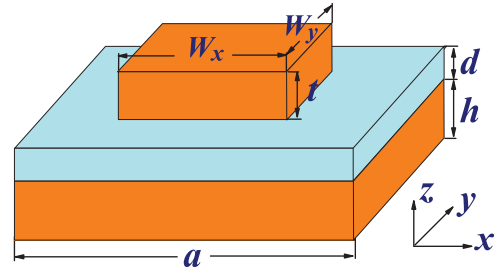

FIG. 1. (Color online) Geometry of the structures studied in this paper. The orange regions are silver, and the cyan region is the dielectric. W_x and W_y represent, respectively, the side lengths of the rectangular metallic particle along the x and y axis and t represents its thickness. d and h, respectively, denote the thicknesses of the dielectric layer and the silver film. a is the lattice constant.

included, namely, $Q_{att} = A + S$. For the perfect metamaterial absorber no transmission signal can be detected owing to the presence of the continuous silver layer. Simultaneously, zero reflectance can also be achieved when the condition perfect impedance matching to the surrounding medium is satisfied. Figure 2(a) shows the simulated reflection and transmission spectra for an absorber with the optimized geometrical parameters. The corresponding attenuation spectrum is presented in Fig. 2(b). As shown in Fig. 2(b), a strong resonance with light attenuation almost 99.9% is observed at the wavelength of 596 nm.
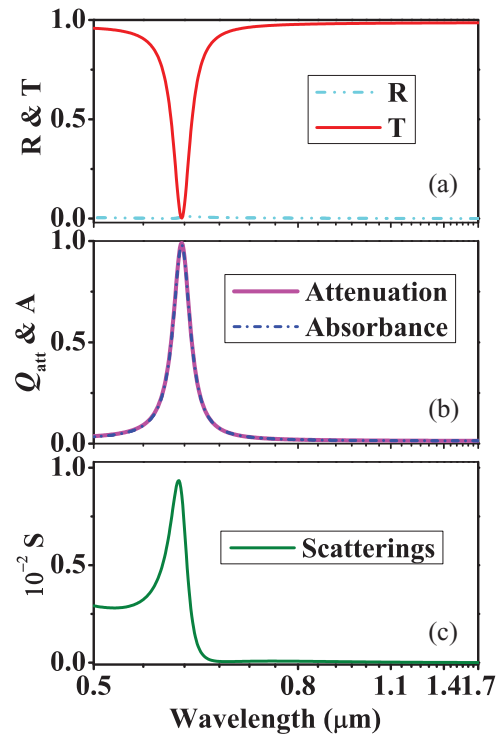

FIG. 2. (Color online) (a) The simulated reflection (R), transmission (T) spectra, (b) correspondingly calculated absorbance (A) and attenuation (Q_{att}) spectra, and (c) the sum of higher-order scattering (S) spectrum for the first kind of metamaterial absorbers.

On the other hand, as was discussed in the Introduction, for such a system the energy of absorbed light ultimately converts into heat; that is,

$$A = Q = \int_V q \, dV. \tag{11}$$

Using Eqs. (9) and (11), we calculate the absorbance for the absorber and plot the result in Fig. 2(b) characterized by the dash-dotted line. It is shown that the feature of absorption spectrum is greatly in accordance with the attenuation spectrum and at the wavelength of 596 nm the absorbance reaches a maximum of 99% as well. The sum of all of high-order scatterings is therefore less than 1% [see Fig. 2(c)]. Consequently, we can confirm that only few incident photons are scattered by the absorber and most of them are indeed absorbed by it. The absorbance can thus be properly calculated using Eq. (10). This is also why all other pervious works can use the formula (10).[29–35],[38,41]

The nature of this type of perfect absorber is very similar to our experimentally demonstrated infrared absorber's.[41] Both are attributed to the excitation of the fundamental electromagnetic resonant mode. The explanation of this fact is that at resonance the localized electromagnetic fields are strongly enhanced, the light energy can be efficiently confined between the metallic particle array, and the bottom metallic layer is then dissipated due to losses.

The widths of the silver particles of the absorber along the different directions are set to be equal, so that the structure is independent of the polarization of normally incident light.[56] In fact, for such a perfect absorber, the absorption effect is also robust for non-normal incident angles. Figure 3 presents the simulated absorbance [calculated using Eq. (10)] as functions of wavelength and the angle of incidence for both TM and TE polarizations. It is found that for TM polarization even for the large oblique incident angle the absorption effect is still very strong, for example, when it is 60° (75°), the absorbance remains 97% (85%). This is due to the fact that the orientation of the magnetic field maintains when the incident angle is varied and it can powerfully keep the strength of magnetic resonance at all of incident angles. For TE polarization, although the absorbance cannot be as high as one for TM polarization, it still remains 87% (58%) at the incident angle 60° (75°). The reason is simply because the orientation of magnetic field does change with the variation of incident angle.

From the macroscopic electromagnetic point of view, our metamaterial perfect absorber with such periodic nanostructures can be interpreted through a homogeneous material characterized by just effective optical parameters: the electric permittivity, ε, and the magnetic permeability, μ.[39,40] Figure 4 shows the retrieved parameters for the present absorber including the effective permittivity, permeability, refractive index, and impedance as well,[57] which were extracted through the inversion of the S parameters [see Figs. 4(a) and 4(b)]. It is found that at the resonant absorption peak wavelength 596 nm the permittivity and permeability take as $\varepsilon = 0.99 + 2.61i$ and $\mu = 1.05 + 2.55i$ (see Case I in Table I), namely, the impedance $Z = \sqrt{\mu}/\sqrt{\varepsilon} = 0.99 - 0.01i$, which is ideally matched to the free space impedance at this wavelength, and then the reflection is negligible. Meanwhile, a nearly perfect
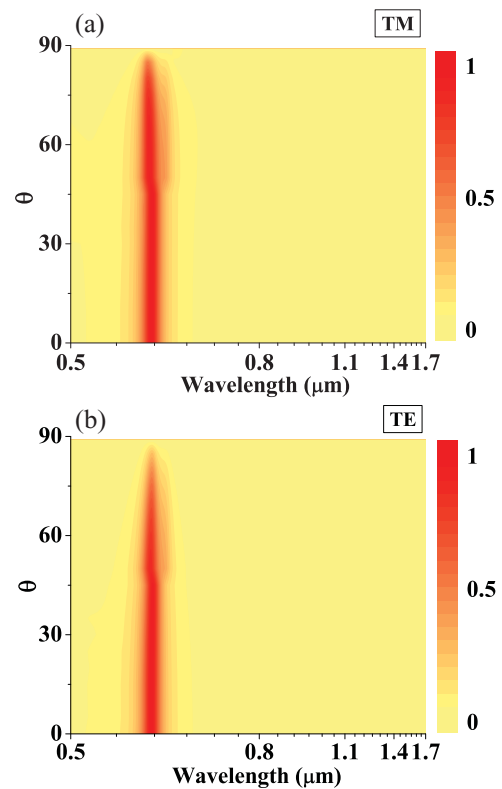

FIG. 3. (Color online) Absorbance as a function of wavelength and the angle of incidence for the first kind of metamaterial absorber. (a) TM polarization; (b) TE polarization.

absorption is achieved as a result of the large imaginary part of the refractive index ($n = \sqrt{\varepsilon}\sqrt{\mu} = 1.02 + 2.58i$).

It is known that the resonance itself does not lead to perfect absorption, because a good matching of impedances must be simultaneously achieved to minimize the reflection. In principle, the impedance at resonance should depend on the dimensions of the structure and the physical properties of the materials. The transmission line modeling[58] is introduced to roughly estimate the effective input impedance of the metamaterial absorber. The impedance is then given by (the details of derivation are presented in supplemental material, Sec. II, which can be found in Ref. 54)

$$Z = j\eta_t \frac{\eta_d \tan(k_d d) + \eta_t \tan(k_t t)}{\eta_t - \eta_d \tan(k_d d) \tan(k_t t)}, \tag{12}$$

where $j = \sqrt{-1}$. $\eta_d = 1/\sqrt{\varepsilon_d}$ and $\eta_t = 1/\sqrt{\varepsilon_t}$ are the characteristic impedances of the dielectric and the layer of silver particle array, respectively. k_d and k_t are the respective wave vector of the two layers. At the resonant absorption wavelength 596 nm, the effective input impedance calculated by Eq. (12) is $Z = 0.85 + 0.07i$, indicating that the condition of impedance matching properly satisfied.

B. Medium-size patches working around their higher-order resonant mode

In this section, we focus on the second kind of metamaterial absorber, which is still working at visible frequency, and more importantly, we investigate the relationship between the absorption spectrum and the geometric dimensions of nanos-
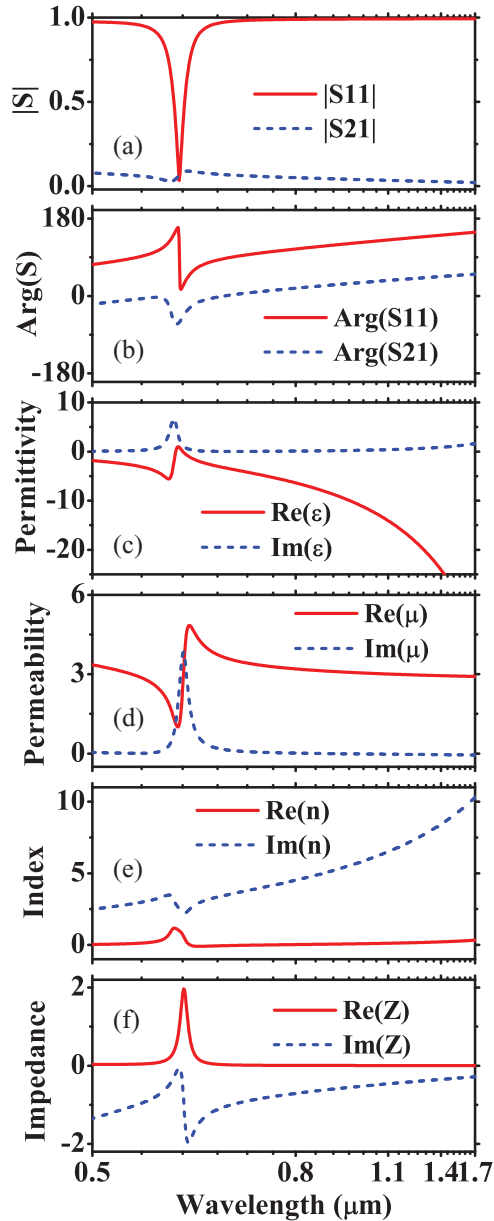
FIG. 4. (Color online) (a) Magnitude and (b) phase of the simulated S parameters for the first kind of metamaterial absorber. Retrieved permittivity (c), permeability (d), refractive index (e), and impedance (f) are also shown.

tructure to illustrate how to design such a high-performance absorber with a set of achievable parameters. Figure 5 presents the absorbance as a function of wavelength and width of the silver particles with other geometric parameters, $t = 30$ nm, $d = 12$ nm, $h = 80$ nm, and $a = 250$ nm, at the normal incidence case. For the sake of simplicity, the widths of the silver particles along the different direction are also assumed to be equal $W_x = W_y = W$ (Ref. 56). As can be observed, the resonant absorption peak can be adjusted over a broad spectral range by changing the width of the metallic particle. Especially, for a wider W, in addition to the absorption band at the long wavelength range associated with the fundamental resonance mode, there exist other absorption bands at shorter wavelengths corresponding to higher-order resonances. For

TABLE I. Effective-medium parameters for the first and second kind of metamaterial absorbers.

	λ_R (nm)	$\varepsilon_{\mathrm{eff}}$	μ_{eff}	n_{eff}	Z_{eff}
I	596	$0.99 + 2.61i$	$1.05 + 2.55i$	$1.02 + 2.58i$	$0.99 - 0.01i$
II	583	$1.03 + 2.45i$	$0.87 + 2.46i$	$0.95 + 2.46i$	$0.99 + 0.03i$

example, when $W = 170$ nm, there is an absorption peak with the center wavelength of 583 nm (which is the third-order mode [denoted by mode (2)] the second-order mode cannot be excited for normally incident light, the reason is discussed below), besides the fundamental mode [denoted by mode (0)] at the wavelength of 1.48 μm. Thus, we can see that the method using higher-order absorption mode can also be used to obtain the high-performance absorber at visible wavelengths with moderate geometric parameters in comparison to using the fundamental mode with much smaller metallic particle. In the following, taking $W = 170$ nm for an example, we present our idea in detail.

Figure 6 shows the simulated reflectance, transmittance, and the corresponding calculated absorbance as functions of wavelength and the thickness of silver film h with other parameters, $W = 170$ nm, $t = 30$ nm, $d = 12$ nm, and $a = 250$ nm, at normal incidence. It is found that the transmission spectrum exponentially decreases when h increases and the reflection signal is always weak and almost independent of the thickness of the continuous silver film. For the present nanostructure dimensions, as h increases from 40 nm, the resonant absorption peak wavelengths (λ_R) for both modes do not change and are located at 583 nm and 1.48 μm, respectively. When $h = 60$ nm, transmittance is much less than 1%. At the wavelength 583 nm (1.48 μm) the skin depth of silver is about 23 nm (22 nm), and thus these results indicate
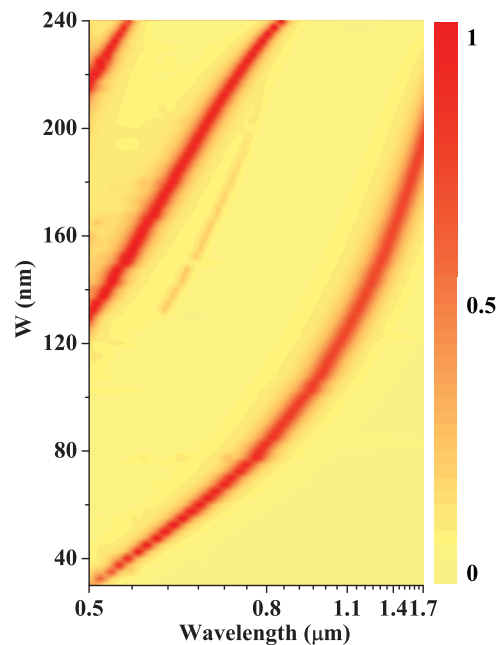

FIG. 5. (Color online) Absorbance as a function of wavelength and the width of the silver particles, where $W_x = W_y = W$, $t = 30$ nm, $d = 12$ nm, $h = 80$ nm, and $a = 250$ nm.
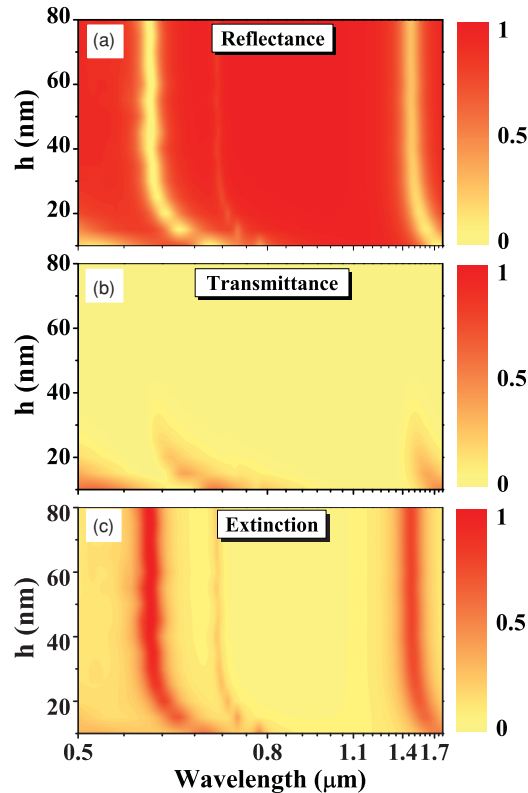
FIG. 6. (Color online) The simulated reflectance, transmittance, and the corresponding calculated absorbance as functions of wavelength and the thickness of silver film h with other parameters $W = 170$ nm, $t = 30$ nm, $d = 12$ nm, and $a = 250$ nm.
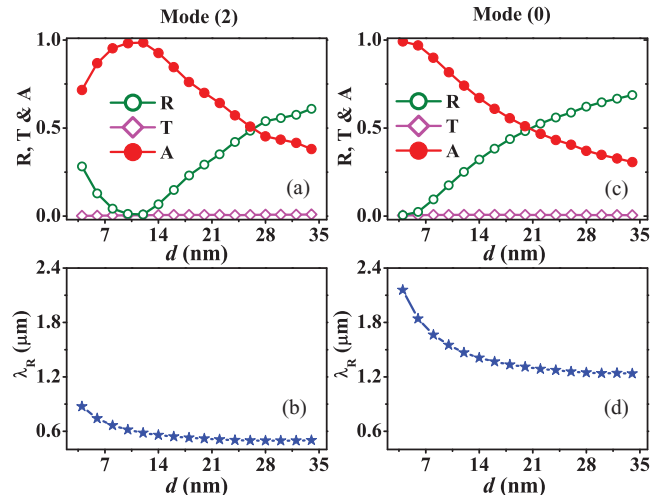

FIG. 7. (Color online) (a) The maximum absorption and correspondingly simulated reflection, with transmission spectra for mode (2) as functions of d with $W = 170$ nm, $t = 30$ nm, $h = 80$ nm, and $a = 250$ nm.(b) The resonant absorption peak wavelength λ_R corresponding to (a) as a function of d. (c) The maximum absorption (A) and correspondingly simulated reflection (R), transmission (T) spectra for mode (0) as functions of d with $W = 170$ nm, $t = 30$ nm, $h = 80$ nm, and $a = 250$ nm. (d) The resonant absorption peak wavelength λ_R corresponding to (c) as a function of d.

that no energy of light can be passed through the structure, as long as h is two times greater than the skin depth. In our simulations, h is set as 80 nm, and much thicker silver film does not play a significant role in the absorption effects. In addition, it is necessary to mention that in comparison to case I using the fundamental mode, the energy of light scattered by this type of absorber increased slightly, but the maximum value does not exceed 4%.

Figure 7(a) presents the evolution of the maximum absorption for mode (2) and correspondingly simulated reflection, with transmission spectra as functions of d with $W = 170$ nm, $t = 30$ nm, $h = 80$ nm, and $a = 250$ nm. The resonant absorption peak wavelength λ_R corresponding to Fig. 7(a) is shown in Fig. 7(b). It is observed that as d increases, the absorption enhances first and approaches to one, then comes down gradually; that is, there exists an optimal thickness d of the dielectric layer that maximizes the absorption. For the present dimensions, when $d = 12$ nm, a resonance with zero reflectance is achieved, and thus a nearly perfect absorber is obtained. This effect is attributed to variation of the near-field plasmon coupling between each silver particle and the continuous silver film. As the dielectric layer thickness increases, the coupling strength increases first until reaching the maximum, then decreases thereafter. When the silver particles are far away from the silver film, the optical properties of such systems are dominantly determined by the film. As a comparison, we also plot the reflection, transmission, and absorption spectra and the corresponding λ_R for mode (0) in Figs. 7(c) and 7(d),

respectively. We find that the optimal thickness is 4 nm for the fundamental mode of the present geometry with resonant wavelength 2.16 μm.

We now perform numerical simulations to investigate the behavior of absorption spectra's dependence on the thickness of silver particle t. Figure 8 shows the simulated results for mode (0) and mode (2), with $W = 170$ nm, $d = 12$ nm, $h = 80$ nm, and $a = 250$ nm. The features of absorption spectra as functions of t for both modes are roughly similar to Figs. 7(a) and 7(b). There exist critical thicknesses corresponding to the maximum absorption. The difference between the modes is that for mode (2) the critical thickness t is 30 nm [Fig. 8(a)] with resonant wavelength λ_R 583 nm [Fig. 8(b)], while it is 15 nm [Fig. 8(c)] with $\lambda_R = 1.67$ μm [Fig. 8(d)] for mode (0). When t decreases from these thicknesses, the intensity of absorption becomes weaker owing to reduction in the plasmon coupling strength between the thinner silver particles and the silver film. For thicknesses larger than these, the absorption also smoothly decreased as t increases. This can be explained as a result of the scattering enhancement of silver particles with the increase in the thickness.

Dependence of the absorption effect on the refractive index of the dielectric layer n_d is also investigated. Figure 9(a) shows the evolution of the maximum absorption for mode (2) and correspondingly simulated reflection, transmission spectra as functions of n_d with dimensions $W = 170$ nm, $t = 30$ nm, $d = 12$ nm, $h = 80$ nm, and $a = 250$ nm. λ_R corresponding to Fig. 9(a) is shown in Fig. 9(b). It appears that the absorption behavior is sensitive to n_d, especially the position of λ_R. The dependency relation between λ_R and index n_d is almost linear within the investigated parameter range and can be fitted by $\lambda_R = 301 \, n_d + 54$, where the dimension for λ_R is nm. This is due to that the refractive index of silver is very linear at
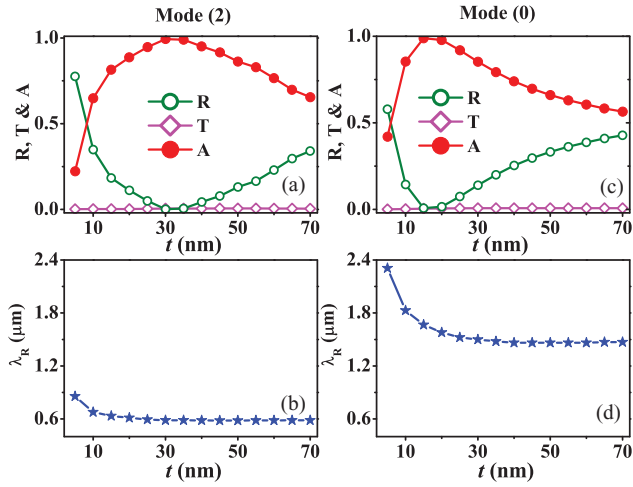
FIG. 8. (Color online) (a) The maximum absorption (*A*) and correspondingly simulated reflection (*R*) and transmission (*T*) spectra for mode (2) as functions of the thickness of silver particles *t* with $W = 170$ nm, $d = 12$ nm, $h = 80$ nm, and $a = 250$ nm. (b) The resonant absorption peak wavelength λ_R corresponding to (a) as a function of *t*. (c) The maximum absorption (*A*) and correspondingly simulated reflection (*R*) and transmission (*T*) spectra for mode (0) as functions of the thickness of silver particles *t* with other geometric parameters $W = 170$ nm, $d = 12$ nm, $h = 80$ nm, and $a = 250$ nm. (d) The resonant absorption peak wavelength λ_R corresponding to (c) as a function of *t*.

this wavelength range.[54] We also find that for mode (0) the tuning sensitivity is even much higher than mode (2) and nearly approaches 700 nm [see Fig. 9(d)]. Nevertheless, to realize a perfect absorbance using the fundamental mode based on the present dimensions, a high n_d of 2.83 is required, and λ_R would be shifted to 2.26 μm, far apart from the visible wavelengths [see Fig. 9(c)].
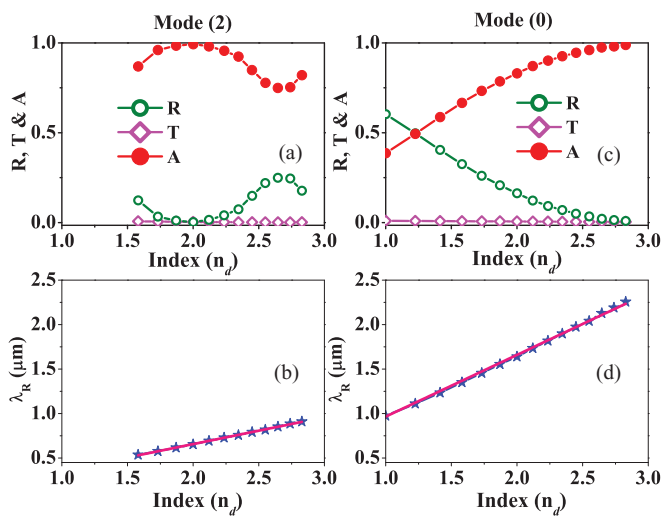

FIG. 9. (Color online) Dependence of the absorption effect on the refractive index of the dielectric layer n_d. (a) Mode (2); (b) the resonant absorption peak wavelength λ_R corresponding to (a); (c) Mode (0); (d) the resonant absorption peak wavelength λ_R corresponding to (c).
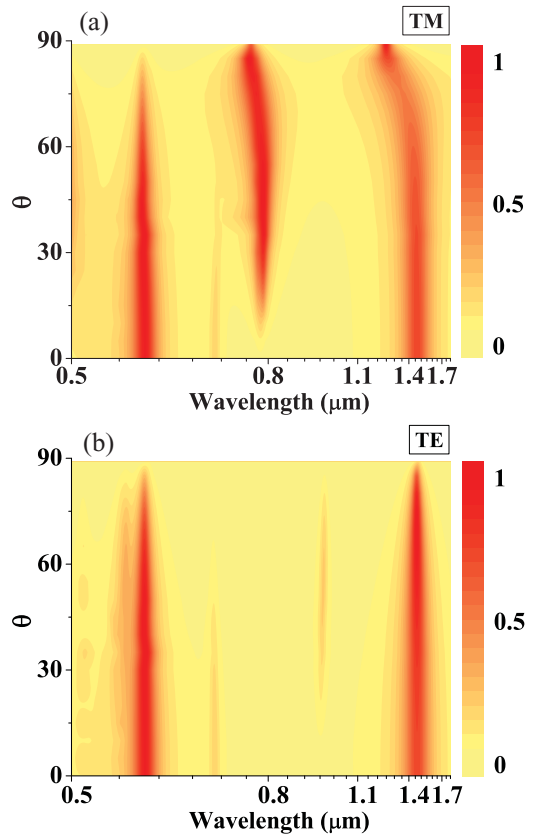

FIG. 10. (Color online) Absorbance as a function of wavelength and the angle of incidence for the second kind of metamaterial absorber: (a) TM polarization; (b) TE polarization.

Further simulations were performed to study the relationship between the absorption and oblique angles of incidence. The simulated absorbance as a function of wavelength for the structure with above optimized parameters is presented in Fig. 10 for both TM [Fig. 10(a)] and TE [Fig. 10(b)] polarizations at various angles of incidence. For mode (2) of each case, the absorption effect is almost independent of angle of incidence. For instance, the absorbance peak is 87% (70%), even with incident angle 60° for TE (TM) polarization. In addition, we find that for TM polarization a new absorption band has arisen between the modes (0) and (2) as the angle of incidence increases. This is exactly the second-order mode [denoted by mode (1)]. To better understand this feature, we also investigate the electromagnetic field distributions for the resonant modes. Figure 11 shows the field distributions for the three modes with wavelengths 583 nm, 787 nm, and 1.48 μm, respectively, calculated by the commercial COMSOL MULTIPHYSICS software based on the three-dimensional finite-elements method. The results at 1.48 μm [Figs. 11(a) and 11(b)] and 583 nm [Figs. 11(g) and 11(h)] are calculated for the normal incident angle while those at 787 nm [Figs. 11(d) and 11(e)] are calculated for an incident angle of 45° (TM polarization). In the field maps of Figs. 11(a), 11(d), and 11(g), the arrows represent electric displacement, whereas the color represents the magnitude of the magnetic field. The electric field distributions for such modes are plotted
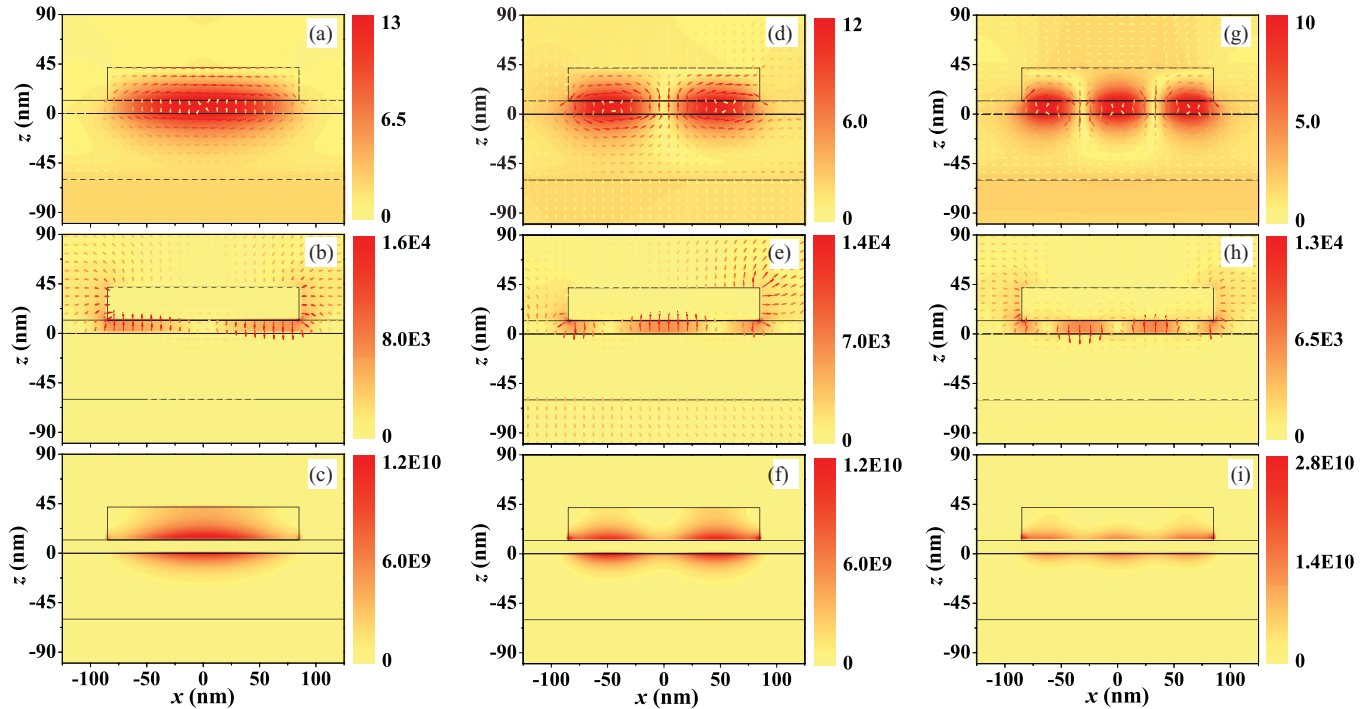
FIG. 11. (Color online) Field distributions and resistive heat for the three modes. (a)–(c) Mode (0) at resonant wavelength 1.48 μm for the normal incident angle. (d)–(f) Mode (1) at resonant wavelength 787 nm for the incident angle of 45°. (g)–(i) Mode (2) at resonant wavelength 583 nm for the normal incident angle. In the field maps of (a), (d), and (g), the arrows represent electric displacement and the color represents the magnitude of the magnetic field. For (b), (e), and (h), the arrows represent the direction of electric field, and the color denotes the magnitude of the electric field. Panels (c), (f), and (i) depict resistive heat corresponding to each case.

in Figs. 11(b), 11(e), and 11(h), respectively. From the field map of Fig. 11(e), we note that the electric field vectors at the center of the spacer layer are exactly perpendicular to the bottom surface of metallic particle. This indicates that to excite the second-order mode, it requires that the electric field of incident light must possess vertical components in the plane of incidence; consequently, we cannot observe the second-order mode at the normal incidence case. For TE modes, the direction of the electric field of incident light remains unchanged with various incident angles and it is always perpendicular to the plane of incidence. This is why TE modes cannot *see* the second mode even for non-normal incident angles.

To better understand the nature of this type of metamaterial absorber based on the microscopic perspective, heat generation in the presence of light radiation is investigated. The time-averaged dissipative energy density for mode (2) is shown in Fig. 11(i). As comparison, we also plot the time-averaged dissipative energy densities for two other modes in Figs. 11(c) and 11(f). Within the investigated wavelength range, the dielectric layer Al$_2$O$_3$ is almost lossless, so for our metamaterial absorber the energy of light is dissipated by the Ohmic losses within the metals. In our simulations, we ignore the temperature effect on the material properties. Suppose the energy density of the incident radiation is 1 mW. The calculated results for mode (2) show that the rate of power dissipation caused by the silver particle is 53.3% and that aroused by the silver film is 43.7%, except 3% of the energy scattered by the system.

In comparison to the energy absorbed by our structure, the scattered energy can be neglected, so that this type of metamaterial absorber can also be described by the effective medium model. We retrieved the effective optical parameters using the simulated transmission and reflection coefficients for normal incident case[57] and plot in Figs. 12(a) and 12(b) the retrieved values of ε and μ. The crucial condition of near-unity
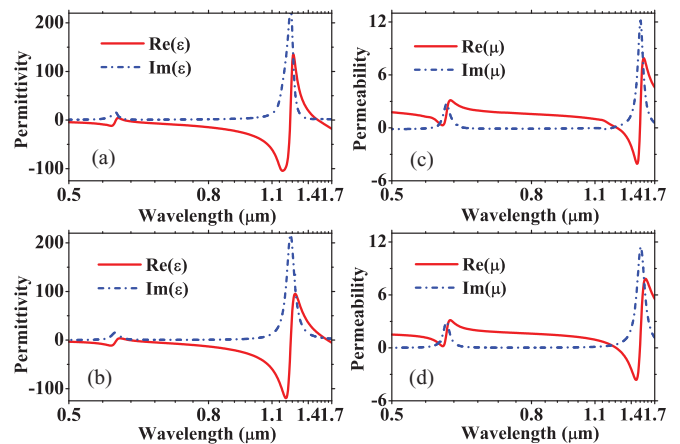

FIG. 12. (Color online) Retrieved effective parameters, (a) permittivity and (b) permeability, for the second kind of metamaterial absorber as functions of wavelength. Optical parameters, (c) permittivity and (d) permeability, calculated with formula (12) as functions of wavelength.

absorption for wavelength 583 nm (see Case II in Table I), impedance matching ($Z = 0.99 + 0.03i$) to free space, and the imaginary part of the refractive index ($n = 0.95 + 2.46i$) as large as possible, are indeed satisfied. Furthermore, we find that the retrieved parameters can be well described by the following Lorentz models:

$$\varepsilon = 4 - \frac{2175^2}{4 \times f^2 + i \times 2 \times f} - \frac{890^2}{f^2 - 243^2 + i \times 15 \times f}$$
$$- \frac{350^2}{f^2 - 525^2 + i \times 15 \times f},$$
$$\mu = 1.8 - \frac{185^2}{f^2 - 202^2 + i \times 15 \times f}$$
$$- \frac{135^2}{f^2 - 514^2 + i \times 15 \times f}, \tag{13}$$

as shown in Figs. 12(c) and 12(d). Here f denotes the frequency in THz. From formulas (12), it is interesting to note that for such a system there really exist a series of electromagnetic resonances associated with high-performance absorption. We also note that the resonant absorption peak wavelength of 583 nm is purely two times larger than the lattice constant (250 nm) of the nanostructures, and conclude that the condition for the validity of effective response functions for our periodic metamaterial structures can be extended significantly beyond the traditional limits of the effective-medium theory.[59,60]

In practice, many factors will affect the quality of the metamaterial absorber fabricated by the state-of-the-art nanofabrication techniques. At the end of this section, we discuss how the presence of fabrication imperfections influences the absorption effect. For example, as shown in Fig. 5, it is found that for a perfect plasmonic metamaterial absorber with the width of the silver particle $W = 170$ nm, the absorbance can be as high as 99% at the wavelength of 583 nm and has a full width at half maximum (FWHM) of 4.6%. If the width displacement of the metamaterial absorber has an amplitude of ± 5 nm (± 10 nm), though the center wavelength of absorption peak does not significantly change, the absorbance would drop to around 80% (70%) and FWHM would become as 8.7% (12.8%). Consequently, the surface roughness and impurities introduced during the fabrication process will contribute to the absorption effect, resulting in decreased resonance strength and spectral broadening.

C. Patches on thick dielectric substrates close to Fabry-Perot condition

The third kind of metamaterial absorber resembles the second one in geometric structure. The difference is the thickness of spacer layer Al_2O_3, which for this type of metamaterial absorber becomes much thicker compared with the other two types. Therefore, this kind of metamaterial absorber possesses the distinct physical origin in absorption effect. The optimized parameters for such an absorber are taken as $W_x = W_y = 150$ nm, $t = 40$ nm, $d = 120$ nm, $h = 80$ nm, and $a = 250$ nm, and the operating wavelength is 595 nm. Figure 13(a) presents the simulated reflection and transmission spectra for the absorber with such the optimal design. We also utilize Eqs. (9) and (11) to calculate the
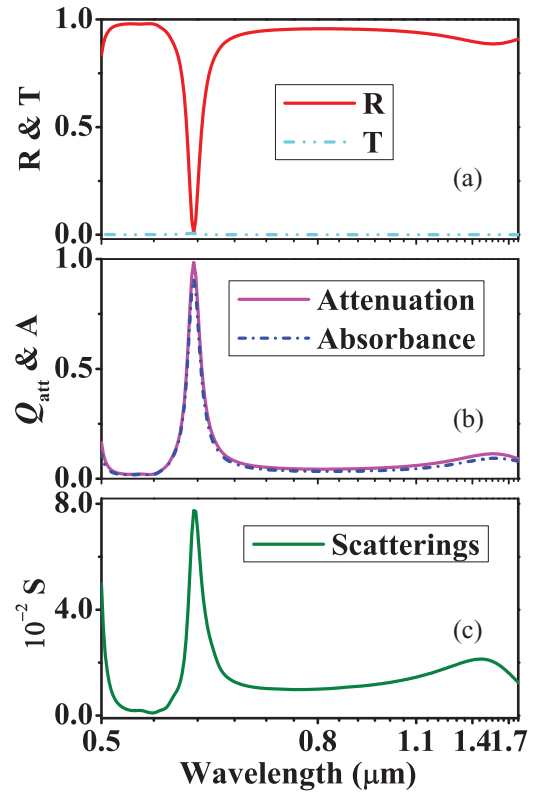

FIG. 13. (Color online) (a) The simulated reflection (R) and transmission (T) spectra, (b) correspondingly calculated absorbance (A) and attenuation (Q_{att}) spectra, and (c) the sum of higher-order scattering (S) spectrum for the third kind of metamaterial absorbers.

absorbance for the absorber and plot the result in Fig. 13(b) as the dash-dotted line. In comparison with the calculated attenuation spectrum based on the simulated reflectance and transmittance, we find that near 8% energy of incident radiation would be scattered by the structure at resonance [see Fig. 13(c)]; the maximum of absorption holds 92%. Although the attenuation spectra contain a part of scattered energy, they are still predominantly attributed to the contributions of absorption. That is, it is appropriate to investigate the absorption properties for the absorber based on the attenuation spectrum.

Figure 14 shows the evolution of the attenuation spectra when the angle of incidence is changed for both TM [Fig. 14(a)] and TE [Fig. 14(b)] polarizations. One can find that the absorption effects for both polarizations are strongly dependent on the angle of incidence. This is due to the thickening of spacer layer Al_2O_3. As a result, the effective thickness of the whole structure gets a high increase, and then leading to the presence of the analog of the Fabry-Perot cavity effect. Such a resonant absorption peak will split into two resonant absorption bands as the the angle of incidence increases. To explore the underlying physics behind this phenomenon, the electromagnetic field distributions for these resonant modes are also investigated. Taking the TM polarization for an example, Fig. 15 shows the field distributions and the time-averaged dissipative energy densities for the three modes with wavelengths 595 nm
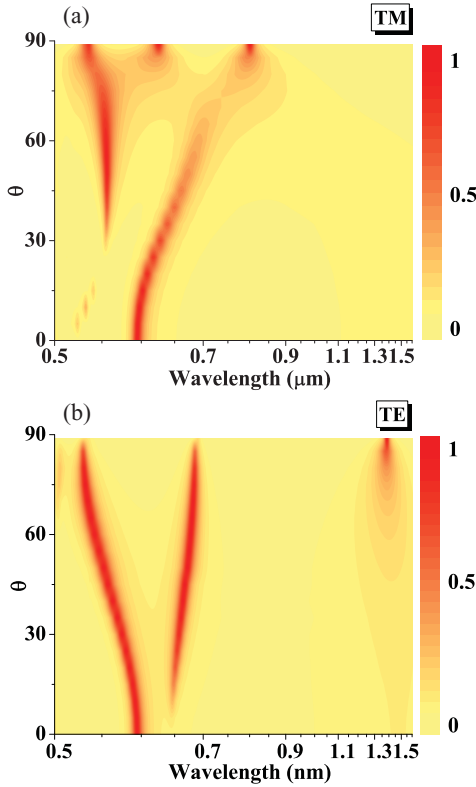
FIG. 14. (Color online) Attenuation as a function of wavelength and the angle of incidence for the third kind of metamaterial absorbers. (a) TM polarization; (b) TE polarization.

FIG. 15. (Color online) Electric (E) and magnetic (H) field distributions and resistive heat (q) for the three modes: (a)–(c) at wavelength 595 nm for the normal incident angle; (d)–(f) at wavelength 691 nm for the incident angle of 60°; (g)–(i) at wavelength 555 nm for the incident angle of 60°.

[Figs. 15(a)–15(c)], 691 nm [Figs. 15(d)–15(f)] and 555 nm [Figs. 15(g)–15(i)], respectively. The results at 595 nm are calculated for the normal incident angle, and these results at 691 and 555 nm are calculated for an incident angle of 60°. From Figs. 15(a)–15(c), one can see that the electromagnetic fields are not only confined to the region below the silver particles, but are also strongly present around the surface of silver film between the silver particles. (The magnetic field intensity enhancement factor is about 130 in comparison with the one in free space at the same situation.) The silver particles and the continuous silver film contributed almost equally to the absorption effect for the normal incidence case. For the off-normal incidence 60° at the resonant wavelength 691 nm, the electromagnetic fields are mostly confined in the region around the surface of silver film between the silver particles; this indicates that the silver film plays the key role in the absorption effect [see Fig. 15(f)]. However, for the another absorption band with the same incident angle 60° at 555 nm, a strong enhancement of electromagnetic field can be merely found in the region around the silver particles; therefore, the heat generation properties of this case are dominantly governed by such particles [see Fig. 15(i)]. Actually, it is not difficult to understand these features. Owing to the thickening of spacer layer Al_2O_3, the condition of the subwavelength for the whole structure is broken, and then the system cannot be regarded as a good homogeneous effective medium. The optical properties determined by part
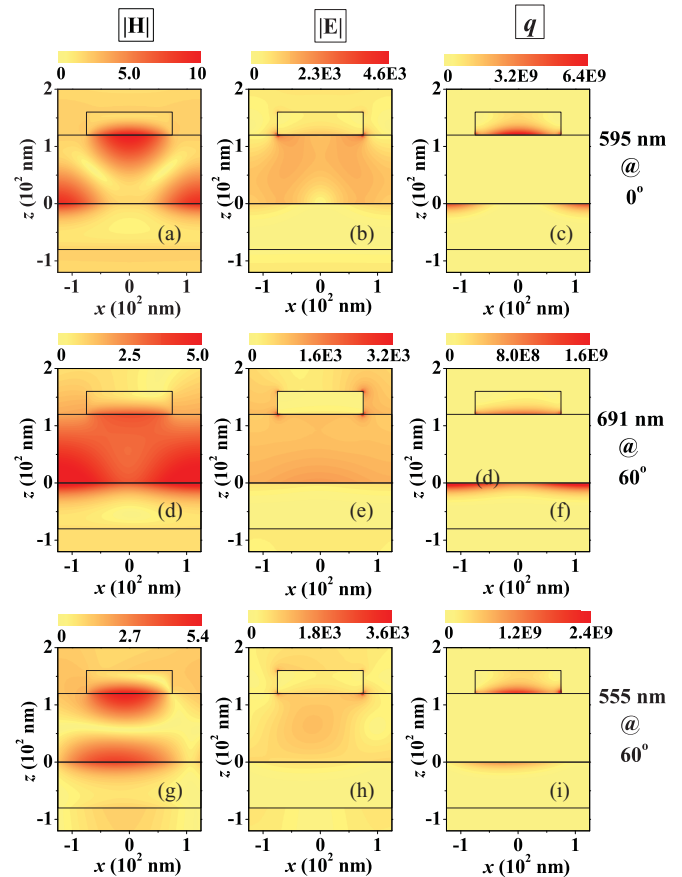
of system will be detected under some specific optical illumination.

IV. CONCLUSIONS

In summary, we have theoretically and numerically studied three kinds of plasmonic metamaterial absorbers for visible frequencies. They resemble each other in geometric structure. All of them are composed of a layer of silver particle array and a continuous of silver film, separated by a dielectric layer. For the first set of metamaterial absorber, which has relatively small silver particles, its high absorption effect is attributed to the excitation of the fundamental electromagnetic resonant mode and insensitive to the angle of incidence. For the second kind of metamaterial absorber, which possesses moderate-size silver particles, its absorption behavior is related to higher-order resonant mode and almost independent of the angle of incidence. The third kind of metamaterial absorber, which has a thicker dielectric layer in comparison with the other two types, presents a distinct absorption phenomenon. The absorption effects are very sensitive to the angle of incidence. Two distinct absorption bands have been observed when the angle of incidence increased. Taking the second

kind of metamaterial absorbers for an example, we performed numerical computations to investigate the relationship between the absorption effect and the geometric dimensions of nanostructure; simulated results show that the absorption spectrum in operating frequency regime can be controlled by adjusting the nanostructure dimensions. Based on Poynting's theorem, we have also studied the heat-loss effect in the medium with both the dispersive and the absorptive dielectric permittivity and magnetic permeability. Using the general resistive heat formula, we investigated the heat generation in all the metamaterial absorbers in order to understand the nature of such high-performance absorption effects. Effective-medium approaches are also employed to describe the absorption properties of the first two kinds of metamaterial absorbers based upon the macroscopic perspective.

---

*Author to whom correspondence should be addressed: min@kth.se

[1] M. Planck, Ann. Phys. D **4**, 553 (1901).

[2] M. Planck, *The Theory of Heat Radiation* (Dover, New York, 1959).

[3] Y. Ahn, J. Dunning, and J. Park, Nano Lett. **5**, 1367 (2005).

[4] Y. Gu, E.-S. Kwak, J. L. Lensch, J. E. Allen, T. W. Odom, and L. J. Lauhon, Appl. Phys. Lett. **87**, 043111 (2005).

[5] O. Hayden, R. Agarwal, and C. M. Lieber, Nat. Mater. **5**, 352 (2006).

[6] P. L. Richards, J. Appl. Phys. **76**, 1 (1994).

[7] X. L. Liu, T. Starr, A. F. Starr, and W. J. Padilla, Phys. Rev. Lett. **104**, 207403 (2010).

[8] T. J. Coutts, Renewable Sustainable Energy Rev. **3**, 77 (1999).

[9] S. Y. Lin, J. Moreno, and J. G. Fleming, Appl. Phys. Lett. **83**, 380 (2003).

[10] H. Sai and H. Yugami, Appl. Phys. Lett. **85**, 3399 (2004).

[11] M. Law, L. E. Greene, J. C. Johnson, R. Saykally, and P. D. Yang, Nat. Mater. **4**, 455 (2005).

[12] B. Tian, X. L. Zheng, T. J. Kempa, Y. Fang, N. F. Yu, G. H. Yu, J. L. Huang, C. M. Lieber, Nature (London) **449**, 885 (2007).

[13] E. Rephaeli and S. Fan, Opt. Express **17**, 15145 (2009).

[14] F. J. García-Vidal, J. M. Pitarke, and J. B. Pendry, Phys. Rev. Lett. **78**, 4289 (1997).

[15] Z. P. Yang, L. J. Ci, J. A. Bur, S. Y. Lin, and P. M. Ajayan, Nano Lett. **8**, 446 (2008).

[16] V. G. Kravets, F. Schedin, and A. N. Grigorenko, Phys. Rev. B **78**, 205405 (2008).

[17] V. Yannopapas, A. Modinos, and N. Stefanou, Opt. Quantum Electron. **34**, 227 (2002).

[18] V. Yannopapas, Phys. Rev. B **73**, 113108 (2006).

[19] V. G. Kravets, S. Neubeck, A. N. Grigorenko, and A. F. Kravets, Phys. Rev. B **81**, 165401 (2010).

[20] R. Wood, Philos. Mag. **4**, 396 (1902); **38**, 98 (1919).

[21] U. Fano, J. Opt. Soc. Am. **31**, 213 (1941).

[22] W. L. Barnes, A. Dereux, and T. W. Ebbesen, Nature (London) **424**, 824 (2003).

[23] F. Z. Yang, J. R. Sambles, and G. W. Bradberry, Phys. Rev. B **44**, 5855 (1991).

[24] K. R. Catchpole and A. Polman, Opt. Express **16**, 21793 (2008).

[25] H. R. Stuart and D. G. Hall, Appl. Phys. Lett. **73**, 3815 (1998).

[26] W. C. Tan, J. R. Sambles, and T. W. Preist, Phys. Rev. B **61**, 13177 (2000).

[27] J. Le Perchec, P. Quémerais, A. Barbara, and T. López-Ríos, Phys. Rev. Lett. **100**, 066408 (2008).

[28] E. Popov, D. Maystre1, R.C. McPhedran, M. Nevière, M. C. Hutley, and G. H. Derrick, Opt. Express **16**, 6146 (2008); E. Popov, S. Enoch, and N. Bonod, *ibid.* **17**, 6770 (2009).

[29] N. I. Landy, S. Sajuyigbe, J. J. Mock, D. R. Smith, and W. J. Padilla, Phys. Rev. Lett. **100**, 207402 (2008).

[30] N. I. Landy, C. M. Bingham, T. Tyler, N. Jokerst, D. R. Smith, and W. J. Padilla, Phys. Rev. B **79**, 125104 (2009).

[31] H. Tao, N. I. Landy, C. M. Bingham, X. Zhang, R. D. Averitt, and W. J. Padilla, Opt. Express **16**, 7181 (2008).

[32] H. Tao, C. M. Bingham, A. C. Strikwerda, D. Pilon, D. Shrekenhamer, N. I. Landy, K. Fan, X. Zhang, W. J. Padilla, and R. D. Averitt, Phys. Rev. B **78**, 241103(R) (2008).

[33] M. Diem, T. Koschny, and C. M. Soukoulis, Phys. Rev. B **79**, 033101 (2009).

[34] Y. Avitzour, Y. A. Urzhumov, and G. Shvets, Phys. Rev. B **79**, 045131(2009).

[35] C. Wu, Y. Avitzour, and G. Shvets, Proc. SPIE **7029**, 70290W (2008).

[36] C. Argyropoulos, E. Kallos, Y. Zhao, and Y. Hao, Opt. Express **17**, 8467 (2009).

[37] Ng Jack, H. Y. Chen, and C. T. Chan, Opt. Lett. **34**, 644 (2009).

[38] N. Liu, M. Mesch, T. Weiss, M. Hentschel, and H. Giessen, Nano Lett. **10**, 2342 (2010).

[39] D. R. Smith, W. J. Padilla, D. C. Vier, S. C. Nemat-Nasser, and S. Schultz, Phys. Rev. Lett. **84**, 4184 (2000).

[40] D. R. Smith, J. B. Pendry, and M. C. K. Wiltshire, Science **305**, 788 (2004).

[41] J. M. Hao, J. Wang, X. L. Liu, W. J. Padilla, L. Zhou, and M. Qiu, Appl. Phys. Lett. **96**, 251104 (2010).

[42] H. H. Richardson, M. T. Carlson, P. J. Tandler, P. Hernandez, and A. O. Govorov, Nano Lett. **9**, 1139 (2009).

[43] G. Baffou, R. Quidant, and F. J. G. de Abajo, ACS Nano **4**, 709 (2010).

[44] G. Baffou, C. Girard, and R. Quidant, Phys. Rev. Lett. **104**, 136805 (2010).

[45] G. L. Liu, J. Kim, Y. Lu, and L. P. Lee, Nat. Mater. **5**, 27 (2006).

[46] L. Cao, D. Barsic, A. Guichard, and M. Brongersma, Nano Lett. **7**, 3523 (2007).

[47] A. M. Gobin, M. H. Lee, N. J. Halas, W. D. James, R. A. Drezek, and J. L. West, Nano lett. **7**, 1929 (2007).

[48] W. Zhao and J. M. Karp, Nat. Mater. **8**, 453 (2009).

[49] A. O. Govorov, and H. H. Richardson, Nano Today **2**, 30 (2007).

[50] G. Baffou, R. Quidant, and C. Girard, Appl. Phys. Lett. **94**, 153109 (2009).

[51] J. D. Jackson, *Classical Electrodynamics*, 3rd ed. (Wiley, New York, 1999).

[52] R. Rupppin, Phys. Lett. A **299**, 309 (2002).

[53] R. Loudon, J. Phys. A **3**, 233 (1970).

[54] P. B. Johnson, and R. W. Christy, Phys. Rev. B **6**, 4370 (1972); see supplemental material at [http://link.aps.org/supplemental/10.1103/PhysRevB.83.165107] for Fig. S1.

[55] A. Taflove, *Computational Electrodynamics: The Finite-Difference-Time-Domain Method* (Artech House INC, Norwood, 2000).

[56] Based on the numerical computational efforts, we find that if the square-shape silver particles of metamaterial absorbers are replaced by the circular silver disks with the same thicknesses and surface areas, the metamaterial absorbers can offer the similar absorption effects.

[57] D. R. Smith, S. Schultz, P. Markos, and C. M. Soukoulis, Phys. Rev. B **65**, 195104 (2002).

[58] Jin Au Kong, *Electromagnetic Wave Theory* (EMW, Cambridge, MA, 2000).

[59] D. R. Smith, D. C. Vier, Th. Koschny, and C. M. Soukoulis, Phys. Rev. E **71**, 036617 (2005).

[60] G. Dolling, M. Wegener, C. M. Soukoulis, and S. Linden, Opt. Lett. **32**, 53 (2007).